

MODEL-PRESERVING ADAPTIVE ROUNDING

Albert Tseng

Cornell University

albert@cs.cornell.edu

Zhaofeng Sun

Cornell University

zs453@cornell.edu

Christopher De Sa

Cornell University

cdesa@cs.cornell.edu

ABSTRACT

The goal of quantization is to produce a compressed model whose output distribution is as close to the original model’s as possible. To do this tractably, most quantization algorithms minimize the immediate activation error of each layer as a proxy for the end-to-end error. However, this ignores the effect of future layers, making it a poor proxy. In this work, we introduce Yet Another Quantization Algorithm (YAQA), an adaptive rounding algorithm that directly considers the error at the network’s output. YAQA introduces a series of theoretical results that culminate in the first end-to-end error bounds for quantization algorithms. First, we characterize the convergence time of adaptive rounding algorithms via the structure of their Hessian approximations. We then show that the end-to-end error can be bounded by the approximation’s cosine similarity to the true Hessian. This admits a natural Kronecker-factored approximation with corresponding near-optimal Hessian sketches. YAQA is provably better than GPTQ/LDLQ and empirically reduces the error by $\approx 30\%$ over these methods. YAQA even achieves a lower error than quantization aware training. This translates to state of the art performance on downstream tasks, all while adding no inference overhead.

1 INTRODUCTION

Modern large language models (LLMs) contain billions of parameters, posing challenges for efficient deployment (Team et al., 2025). One way to improve the cost-benefit tradeoffs of LLM inference is by quantizing high precision model parameters θ^* to low precision representations. In memory-bound settings, this reduces bandwidth, and in compute-bound settings, hardware-supported datatypes increase throughput. At their core, quantization frameworks (e.g. QuIP#) consist of two components: a quantizer \mathcal{Q} (e.g. E8P) that defines a set of representable points C , and a rounding algorithm (e.g. LDLQ) that assigns $\theta^* \rightarrow C$. While quantizers are restricted by inference constraints, rounding algorithms give flexibility in the final model.

The goal of a rounding algorithm is to best preserve the original model outputs:

$$\hat{\theta} \leftarrow \arg \min_{\theta \in C} \mathbb{E}_{X \sim \mathcal{D}} [D_{\text{KL}}(M(\theta^*, X) \| M(\theta, X))], \quad (1)$$

where M is a model architecture, $M(\theta^*, X)$ are the original model outputs, $M(\theta, X)$ are the quantized model outputs, and X is a input example sampled from a data distribution \mathcal{D} . Exactly solving the problem in Equation 1 is intractable due to the combinatorial nature of discrete optimization. Instead, state-of-the-art quantization frameworks either optimize Equation 1 with first-order descent-style methods such as quantization aware training (QAT), or second-order adaptive rounding algorithms such as GPTQ (Team et al., 2025; Frantar et al., 2023). The former requires significant amounts of compute to “learn” quantized representations, and the latter algorithmically rounds individual layers with second-order statistics.

To round a layer with second-order statistics, let $\mathcal{L}(W)$ denote the loss of Equation 1 resulting from changing that layer’s weights to W , leaving all other weights alone with their value in θ^* . Then,

$$\mathcal{L}(W) \approx \frac{1}{2} \text{vec}(W - W^*)^T (\nabla^2 \mathcal{L}(W^*)) \text{vec}(W - W^*), \quad (2)$$

where $W^* \in \mathbb{R}^{m \times n}$ are the original weights and first order terms involving $\nabla \mathcal{L}(W^*)$ are 0 since D_{KL} is minimized at the original model. Note that this is just a standard second order approximation of the

end-to-end loss for a single layer. Since $\nabla^2 \mathcal{L}(W^*) \in \mathbb{R}^{mn \times mn}$ is too large to directly operate on, modern adaptive rounding algorithms use information from structured approximations (colloquially “Hessians”) of $\nabla^2 \mathcal{L}(W^*)$ to round elements of W^* .

For example, the widely used GPTQ algorithm rounds using the Hessian of the immediate layerwise activation error as a proxy for $\nabla^2 \mathcal{L}(W^*)$ (Frantar et al., 2023). Like with \mathcal{L} , the minimum of this objective is achieved at the original model, but since this ignores the effect of quantization on future layers, it is not a very good proxy. Newer methods such as GuidedQuant and SqueezeLLM have explored using block diagonal approximations of the empirical Fisher to incorporate additional information from $\nabla^2 \mathcal{L}(W^*)$ Kim et al. (2025; 2023). Unfortunately, these structured approximations are largely ad-hoc, with little theoretical justification for either the structure or approximation used.

This begs the question: *what fundamental properties of Hessian sketches admit tractable adaptive rounding algorithms that produce high quality models?* In this work, we answer with Yet Another Quantization Algorithm (YAQA), an new adaptive rounding algorithm that, *for the first time ever, comes with bounds on the end-to-end quantization error*. YAQA generalizes LDLQ to consider the full model error, and is provably better at minimizing the KL while having the same asymptotic cost.

YAQA relies on a few key theoretical insights. We first characterize the convergence time of LDLQ and show that for it to be tractable, the Hessian approximation must have certain structural properties. This gives rise to a natural Kronecker-factored Hessian approximation that admits symmetric input and output-side feedback during rounding. Then, we show that the KL of YAQA’s adaptive rounding algorithm can be bounded by the cosine similarity between its Hessian and $\nabla^2 \mathcal{L}(W^*)$. This motivates YAQA’s Hessian sketches, which power iterate on $\nabla^2 \mathcal{L}(W^*)$ to obtain near-optimal Hessians. Empirically, YAQA reduces the KL by $\approx 30\%$ over LDLQ, achieves a lower KL than QAT, and sets a new state of the art in PTQ quality. In summary, we:

1. Introduce YAQA, a new quantization algorithm that generalizes local adaptive rounding methods to optimize the end-to-end KL and is provably better than GPTQ and LDLQ.
2. Characterize desiderata for Hessian sketches that simultaneously admit tractable adaptive rounding algorithms and high quality quantized models and prove the first ever theoretical bounds on the end-to-end quantization error.
3. Show that YAQA achieves a significantly lower empirical KL than existing rounding algorithms, including large-scale QAT, and achieves state of the art downstream results.

2 BACKGROUND

2.1 LARGE LANGUAGE MODEL QUANTIZATION

LLM quantization approaches largely fall into two categories: post-training quantization (PTQ) and quantization aware training (QAT). In PTQ, models are compressed after training, whereas QAT and low-precision training methods produce *natively quantized models* through modified training recipes (Nagel et al., 2022; Tseng et al., 2025). Although PTQ has achieved popularity due to its combination of strong quality and relatively low cost, QAT can produce better models at the expense of needing significantly more compute. However, PTQ and QAT are not completely orthogonal. Recently, a class of PTQ approaches has emerged where weights are “learned” over a restricted subspace. For example, DiscQuant performs descent on the full model KL but limits parameters to either be rounded up or down, and PV-Tuning only optimizes a select subset of parameters at any given step (Chee et al., 2025; Malinovskii et al., 2024).

2.1.1 LOCAL LAYERWISE ROUNDING

Most quantization algorithms use H_1 , the Hessian of the immediate activation error ($\|x(W - W^*)^T\|_F^2$), as an approximation of $\nabla^2 \mathcal{L}(W^*)$. $H_1 \in \mathbb{R}^{n \times n} = \mathbb{E}[x^T x]$, where $x \in \mathbb{R}^{1 \times n}$ is the input activation to that layer and the expectation is taken over some data distribution. H_1 can be computed with only forward passes, making it cheap to obtain. In GPTQ and LDLQ, which are equivalent, columns in W^* are iteratively rounded with linear feedback from the Cholesky decomposition of H_1 . For the rest of this paper, we use LDLQ’s presentation from Chee et al. (2023) to refer to both. In AWQ, input channels are weighted with the diagonal of H_1 (Lin et al., 2023). Chee et al. (2023)

showed that the error of LDLQ could be bounded by an increasing function of H_1 ’s incoherence, which intuitively measures how uniform important rounding directions are.

Definition 1 (Chee et al. (2023)). *A Hessian $H \in \mathbb{R}^{n \times n}$ is μ -incoherent if its eigendecomposition $H = Q\Lambda Q^T$ has $\max_{i,j} |Q_{ij}| = \max_{i,j} |e_i^T Q e_j| \leq \mu/\sqrt{n}$.*

To reduce μ for H_1 , Chee et al. (2023) introduced *incoherence processing*, which concentrates H_1 and W^* by fast random orthogonal transformations. In QuIP#, Tseng et al. (2024a) did this with the randomized Hadamard transform (RHT), which also makes W approximately Gaussian.

2.1.2 FULL MODEL ADAPTIVE ROUNDING

Since H_1 ignores the effect of future layers on quantization, quantizing with H_1 does not always reduce the KL. Methods such as OBS, AdaRound, SqueezeLLM, and GuidedQuant have explored using additional information from the *empirical* Fisher matrix on the task loss (next-token cross entropy), which is fundamentally different from $\nabla^2 \mathcal{L}(W^*)$ (Hassibi et al., 1993; Nagel et al., 2020; Kim et al., 2023; 2025; Kunstner et al., 2020). These methods assume the model is trained to convergence, which is almost never true for LLMs (Hoffmann et al., 2022), and use block diagonal approximations to maintain tractability. Although these methods can outperform LDLQ, they do not generally come with error bounds, making it difficult to reason about their characteristics. Furthermore, their Hessian sketches are largely ad-hoc, making it unclear if the resulting approximation is good or not. For example, increasing the fidelity of GuidedQuant’s Hessian approximation does not consistently reduce the error. In contrast, as we show in Section 3.1, YAQA’s KL can be bounded by the cosine similarity between its Hessian and $\nabla^2 \mathcal{L}(W^*)$, which YAQA maximizes by construction.

2.1.3 GRADIENT-DESCENT-BASED METHODS

In all the aforementioned methods, quantized representations are obtained without “learning” and are not updated once they are obtained. In contrast, certain recent algorithms perform what is essentially constrained QAT with a much smaller compute budget. In PV-Tuning, learnable codebooks and code assignments are jointly optimized to minimize the end-to-end KL (Malinovskii et al., 2024). In DiscQuant, model weights are updated with gradient descent in a constrained subspace (Chee et al., 2025). In CBQ, quantized weights are learned with LoRA adapters and regularization in an AdaRound-style setup (Ding et al., 2025). In general, these methods are restricted to suboptimal scalar or unstructured vector quantizers. Finally, although some of these methods are guaranteed to perform local descent, QAT in general is not a descent method, making it hard to characterize.

2.2 HESSIAN APPROXIMATIONS

While quantization works have mostly used H_1 or block diagonal Hessian approximations, prior *optimization* works have proposed a wide variety of Kronecker-factored Hessian sketches ($H \approx H_O \otimes H_I$) in the context of learning algorithms. Most sketches are based off the Fisher Information Matrix $\mathbb{E}[\text{vec}(\nabla_{W^*} \ell) \text{vec}(\nabla_{W^*} \ell)^T]$. In the real Fisher, which is equal to $\nabla^2 \mathcal{L}(W^*)$ (Gourieroux & Monfort, 1995), ℓ is computed with a Monte-Carlo sample over the model output logits. In the empirical Fisher, ℓ is the next token cross entropy. In KFAC, the authors show that for linear layers in MLPs, $H = \mathbb{E}[x^T x \otimes (\nabla_y \ell)^T (\nabla_y \ell)]$, which gives the approximation $H_I = \mathbb{E}[x^T x]$ and $H_O = \mathbb{E}[(\nabla_y \ell)^T (\nabla_y \ell)]$ (Martens & Grosse, 2015). In Shampoo, the authors propose approximating the empirical Fisher with $H_I = \mathbb{E}[(\nabla_{W^*} \ell)^T (\nabla_{W^*} \ell)]$, $H_O = \mathbb{E}[(\nabla_{W^*} \ell) (\nabla_{W^*} \ell)^T]$ (Gupta et al., 2018). Finally, other works have proposed “eigencorrected” versions of these approximations (George et al., 2018; Vyas et al., 2025), which are beyond this discussion.

3 YET ANOTHER QUANTIZATION ALGORITHM

Here, we describe YAQA, a layerwise adaptive rounding method that rounds layers to minimize the full model KL divergence. YAQA consists of two components: 1) a theoretically principled rounding algorithm that generalizes LDLQ to consider the full model error, and 2) a series of near-optimal Hessian sketches for the rounding algorithm that can be tractably computed for large modern LLMs. Since YAQA only chooses a representation within a quantized space, YAQA can be used with any quantizer and does not affect the inference efficiency of the quantized model.

3.1 END-TO-END LAYERWISE ADAPTIVE ROUNDING

In the state-of-the-art local layerwise adaptive rounding algorithm LDLQ, each linear layer weight matrix $W^* \in \mathbb{R}^{m \times n}$ is independently rounded to produce W with the following fixed point iteration:

$$W = \mathcal{Q}(W^* + (W^* - W)(L_1 - I)), \quad (3)$$

where L_1 is the triangular component of the LDL decomposition of H_1 and specifies linear feedback along the input channels of W^* . Here, \mathcal{Q} is a scalar quantizer; we detail the vector quantization case in the Appendix. LDLQ acts to minimize the loss $\text{tr}((W^* - W)H_1(W^* - W)^T)$, which is a proxy for the end-to-end error $\mathcal{L}(W)$ in Equation 2.

We want to generalize this to other Hessian sketches that result in better quadratic proxy losses for $\mathcal{L}(W)$. In the most general case, consider a Hessian sketch $\tilde{H} \in \mathbb{R}^{mn \times mn}$ with LDL decomposition $\tilde{H} = LDL^T$ and the fixed-point iteration

$$W = \text{vec}^{-1}(\mathcal{Q}(\text{vec}(W^*) + \text{vec}(W^* - W)(L - I))), \quad (4)$$

where vec^{-1} returns to the original shape. This update, which requires $\mathcal{O}(m^2n^2)$ operations as written, is obviously intractable in general: we are interested in characterizing cases where the *structure* of \tilde{H} allows adaptive rounding to be efficient.

3.1.1 WHEN IS ADAPTIVE ROUNDING FAST?

For Equation 4 to be fast, we need two properties to hold. First, L must admit fast matrix-vector multiplication in $o(m^2n^2)$ time. Second, the fixed-point iteration should terminate in a small number of steps. Structured matrices that satisfy the former have been well-studied (De Sa et al., 2017), so we focus on the latter. The key property we need is a metric we call the “structural nilpotence degree”:

Definition 2 (Structural Nilpotence Degree (SND)). *Let L be a unit triangular matrix. $\text{snd}(L)$ is the degree of the binary nilpotent matrix N with the same support (nonzero mask) as $L - I$.*

The SND bounds the number of steps Equation 4 needs to converge, which follows from observing that $N = L - I$ is the adjacency matrix of the dependency graph of the update in Equation 4.

Lemma 1. *Equation 3 converges after at most $\text{snd}(L)$ steps.*

It is straightforward to see that for a general dense lower triangular $L \in \mathbb{R}^{mn \times mn}$, $\text{snd}(L) = mn$, which matches our earlier analysis of running LDLQ on \tilde{H} and $\text{vec}(W^*)$. Lemma 1 reduces the problem of finding an approximation of H that makes LDLQ tractable to finding one with fast matrix-vector multiplication and low SND. This next lemma helps us do that.

Lemma 2. *Let L_1, L_2 be unit triangular matrices. Then $\text{snd}(L_1 \otimes L_2) = \text{snd}(L_1) + \text{snd}(L_2)$.*

This result motivates us to use a Kronecker-factored approximation $\tilde{H} = H_O \otimes H_I$, for $H_O \in \mathbb{R}^{m \times m}$ and $H_I \in \mathbb{R}^{n \times n}$, in YAQA. Since the LDL decomposition of this \tilde{H} is $H_O \otimes H_I = (L_O \otimes L_I)(D_O \otimes D_I)(L_O \otimes L_I)^T$, where $L_O D_O L_O^T$ is the LDL decomposition of H_O and likewise for H_I , it follows that for $L = L_O \otimes L_I$, $\text{snd}(L) = \text{snd}(L_O) + \text{snd}(L_I) \leq m + n - 1$. We can also see that this admits fast multiplication, as running Equation 4 on this \tilde{H} (hereafter called “YAQA”) is equivalent to

$$W = \text{vec}^{-1}(\mathcal{Q}(\text{vec}(W^*) + \text{vec}(\Delta)(L_O \otimes L_I - I))) = \mathcal{Q}(W^* + L_O'^T \Delta L_I' + L_O'^T \Delta + \Delta L_I'), \quad (5)$$

where $L_O' = L_O - I$, $L_I' = L_I - I$, and $\Delta = W^* - W$. This means “YAQA” can run in $m + n$ iterative steps, each of which are mostly highly parallelizable low-dimensional matrix multiplies.

Compared to LDLQ, Equation 5 has two additional components that give “output side” feedback: $L_O'^T \Delta$ and $L_O'^T \Delta L_I'$. This is conceptually nice since the feedback is symmetric across input and output channels. In contrast, GuidedQuant, which can also be expressed in our “SND framework” as running LDLQ on a block-diagonal approximation (see Appendix), uses no output side feedback regardless of the number of blocks. Indeed, GuidedQuant’s performance plateaus after as few as 4 blocks.

3.1.2 END-TO-END ERROR BOUNDS AND HESSIAN DESIDERATA

Like LDLQ, we can bound the proxy error of YAQA $\text{vec}(\Delta) \tilde{H} \text{vec}(\Delta)^T = \text{tr}(\Delta^T H_O \Delta H_I)$ (see Appendix). However, we can also bound the “true second-order error” $\text{vec}(\Delta) H \text{vec}(\Delta)^T$, for the

“true Hessian” $H = \nabla^2 \mathcal{L}(W^*)$, by the proxy error and cosine similarity between $H_O \otimes H_I$ and H , which gives *the first end-to-end error bound for any quantization algorithm*.

Theorem 1. *Let $H \in \mathbb{R}^{mn \times mn} = \nabla^2 \mathcal{L}(W^*)$ be the Hessian of a linear layer W with respect to the KL to the original model outputs, $H_O \in \mathbb{R}^{m \times m}$ and $H_I \in \mathbb{R}^{n \times n}$ be two p.d. matrices, and \mathcal{Q} perform nearest or stoch. rounding with $\mathbb{E}[(\mathcal{Q}(x) - x)^2] \leq \sigma^2$. Furthermore, let W be the output of Equation 5 with L'_O, L'_I from the LDL decompositions of H_O, H_I , respectively. Then,*

$$\text{vec}(\Delta)H \text{vec}(\Delta)^T \leq \|H\|_F \left(\|\Delta\|_F^2 \sqrt{2 - 2c} + \frac{\mu_I^2 \mu_O^2}{mn \|H_I\|_F \|H_O\|_F} \text{tr}(H_I^{1/2})^2 \text{tr}(H_O^{1/2})^2 \sigma^2 \right)$$

where $c = \frac{\langle H, H_O \otimes H_I \rangle}{\|H\|_F \|H_O\|_F \|H_I\|_F}$ is the cosine similarity between H and $H_O \otimes H_I$.

Theorem 1 states two things. First, the closer $H_O \otimes H_I$ is directionally to H , the better YAQA minimizes Equation 2. This intuitively makes sense since H captures the important rounding directions – having an approximation that is directionally similar to H should give a better quantized model. Second, H_O and H_I should both have low incoherence and, as we will show, be approximately low rank. The former follows directly from μ_O and μ_I , and the latter follows from the fact that regular LDLQ is equivalent to YAQA with $H_O = I$ and $H_I = H_1$.

With this equivalence, the ratio between the “trace part” of the bounds for YAQA and LDLQ is

$$\frac{\mu_O^2 \mu_I^2 \text{tr}(H_I^{1/2})^2 \|H_1\| \text{tr}(H_O^{1/2})^2}{m \sqrt{m} \mu_1^2 \text{tr}(H_1^{1/2})^2 \|H_I\| \|H_O\|}. \quad (6)$$

From Cauchy-Schwarz, $\text{tr}(H_O^{1/2})^2 \leq k_O \text{tr}(H_O)$, so if H_O has rank $k_O \leq \frac{m \mu_1^2 \text{tr}(H_1^{1/2})^2 \|H_1\|}{\mu_O^2 \mu_I^2 \text{tr}(H_I^{1/2})^2 \|H_I\|}$ then Equation 6 ≤ 1 . When H_O is low rank, YAQA achieves a lower error bound than LDLQ.

These properties give us a clear objective for constructing a good Kronecker-factored Hessian sketch for YAQA: we wish to maximize c and minimize the incoherences and ranks of H_O, H_I . Although we cannot easily control the rank of either factor, we *can* maximize c with power iteration. Specifically, the Kronecker product is a reshaped rank-1 product (Loan, 2000) so we can find H_O and H_I by power iterating on H . In the following section, we describe how to tractably do so for modern LLMs.

3.2 SCALABLE NEAR-OPTIMAL KRONECKER FACTORED HESSIAN SKETCHES

We wish to find $H_I, H_O = \arg \min_{H_I, H_O} \|H - H_O \otimes H_I\|_F^2$. This can be done with power iteration:

$$(H_I)_i \leftarrow H(H_O)_{i-1} / \|(H_O)_{i-1}\|_F^2 \quad (H_O)_i \leftarrow (H_I)_{i-1} H / \|(H_I)_{i-1}\|_F^2. \quad (7)$$

which is guaranteed to converge to the optimal H_O, H_I . However, power iterating on H is practically difficult. Recall that H is equal to the real Fisher Information Matrix, or $\mathbb{E}[\text{vec}(\nabla_{W^*} \ell) \text{vec}(\nabla_{W^*} \ell)^T]$, where the expectation is taken over independent samples and ℓ is the cross entropy with a Monte-Carlo sample from the output logits. In LLMs, tokens within a sequence are not independent due to sequence mixing (e.g. with attention). As such, H must be computed over *entire sequences and not individual tokens*, which increases the variance of the estimate.

To remedy this, we propose two different Hessian sketches that both have high cosine similarity to H while being tractable. Sketch A assumes tokens are independent within a linear layer, which reduces the variance to $O(1/\#\text{tokens})$ at the cost of a slightly biased estimate. Sketch B runs one round of power iteration on $\nabla^2 \mathcal{L}(W^*)$ starting from an identity initialization, which can be computed in a single pass over a dataset. This lets us use enough sequences to achieve low variance without blowing up cost. We show that given sufficient data, Sketch B both theoretically and empirically outperforms Sketch A. However, both are still significantly better than prior state-of-the-art rounding algorithms.

3.2.1 HESSIAN SKETCH A

Sketch A performs power iteration on a Hessian estimate that assumes that tokens within a sequence are independent. In this setting, $(\nabla^2 \mathcal{L}(W^*))_A = \mathbb{E}_{x \sim D} [x^T x \otimes (\nabla_y \ell)^T (\nabla_y \ell)]$, where ℓ is computed with the same Monte-Carlo sample as before but each x, y pair corresponds to an *individual token*. This sketch is obviously biased but reduces the variance by increasing the sample size to the number of tokens. Furthermore, $(\nabla^2 \mathcal{L}(W^*))_A$ still has sequence information from $(\nabla_y \ell)$, so it is

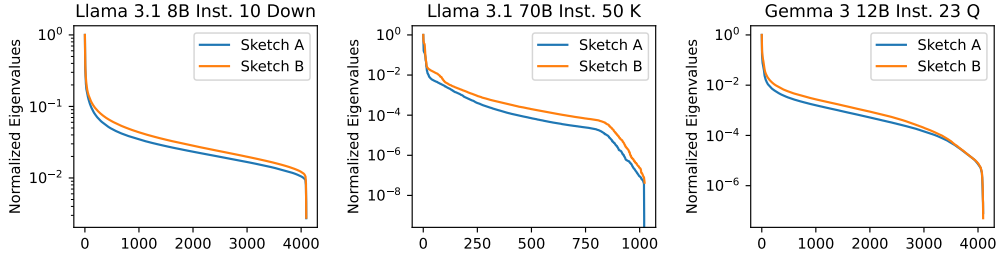


Figure 1: Real-world H_O ’s from A and B are approximately low rank and have similar spectrums.

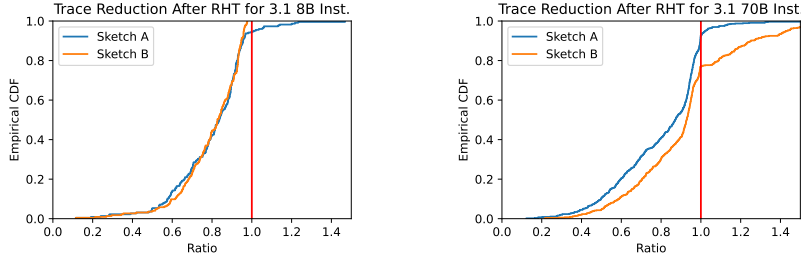


Figure 2: Empirical CDF of $\frac{\text{tr}(D_O^{\text{IP}}) \text{tr}(D_I^{\text{IP}})}{\text{tr}(D_O) \text{tr}(D_I)}$ across linear layers, where D^{IP} denotes D after incoherence processing H with the RHT. A ratio of < 1 (left of the red line) indicates a reduction in error bound.

still empirically close to $\nabla^2 \mathcal{L}(W^*)$. To perform power iteration with $(\nabla^2 \mathcal{L}(W^*))_A$, we compute

$$(H_I)_i \leftarrow \mathbb{E}_{x \sim D} [x^T x \langle (H_O)_{i-1}, (\nabla_y \ell)^T (\nabla_y \ell) \rangle] / \| (H_O)_{i-1} \|_F^2 \quad (8)$$

$$(H_O)_i \leftarrow \mathbb{E}_{x \sim D} [(\nabla_y \ell)^T (\nabla_y \ell) \langle (H_I)_{i-1}, x^T x \rangle] / \| (H_I)_{i-1} \|_F^2. \quad (9)$$

Equations 8 and 9 only require the input x and error signal $\frac{d\ell}{dy}$, so we can use a modified backward pass to perform fully-distributed power iteration. To speed up convergence, we initialize H_O, H_I with the LDLQ Hessian: $(H_I)_0 \leftarrow H_1, (H_O)_0 \leftarrow I$. Empirically, Sketch A converges in ≤ 3 full iterations and takes around 20 GPU-hours for a 10B parameter model and 20M token dataset.

3.2.2 HESSIAN SKETCH B

Sketch B directly computes the result of one round of power iteration on $\nabla^2 \mathcal{L}(W^*)$ starting with $H_I, H_O \leftarrow I$. Observe that power iterating on $\nabla^2 \mathcal{L}(W^*)$ involves computing the following updates

$$(H_I)_i \leftarrow \frac{\mathbb{E}_{s \sim D} [(\nabla_{W^*} \ell)^T (H_O)_{i-1} (\nabla_{W^*} \ell)]]}{\| (H_O)_{i-1} \|_F^2} \quad (H_O)_i \leftarrow \frac{\mathbb{E}_{s \sim D} [(\nabla_{W^*} \ell) (H_I)_{i-1} (\nabla_{W^*} \ell)^T]}{\| (H_I)_{i-1} \|_F^2}. \quad (10)$$

If $(H_I)_0$ and $(H_O)_0$ are both I , then $(H_I)_1 = \mathbb{E}_{s \sim D} [(\nabla_{W^*} \ell)^T (\nabla_{W^*} \ell)] / m$ and $(H_O)_1 = \mathbb{E}_{s \sim D} [(\nabla_{W^*} \ell) (\nabla_{W^*} \ell)^T] / n$, where the expectation and $\nabla_{W^*} \ell$ are computed over sequences. Both of these are computable in the same backward pass, letting us do one round of power iteration on both H_O and H_I in a *single pass over a dataset*. This sketch is conceptually similar to the preconditioning basis in Shampoo (Gupta et al., 2018; Morwani et al., 2025), except that we compute the gradient per-sequence instead of per-batch and use the real Fisher instead of the empirical Fisher. Sketch B takes around 30 GPU-hours for a 10B parameter model and 64K sequences of 2K tokens each.

3.2.3 EVALUATING SKETCH A AND B

In Section 3.1, we desired to find a Kronecker-factored sketch with low rank, low incoherence, and high cosine similarity to the true Hessian. Here, we evaluate how well Sketch A and B achieve these goals. Figure 1 shows that empirically, real-world H_O matrices have strong spectral decay and are approximately low rank. Figure 2 shows the empirical CDF across layers of the ratio $\frac{\text{tr}(D_O^{\text{IP}}) \text{tr}(D_I^{\text{IP}})}{\text{tr}(D_O) \text{tr}(D_I)}$, where D^{IP} denotes D_I after incoherence processing H_I with the RHT and likewise for D_O^{IP} and

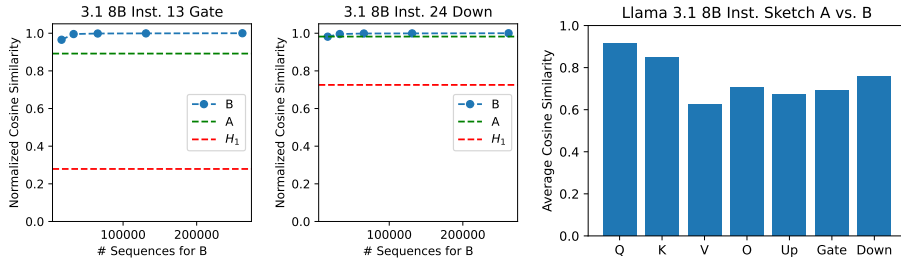


Figure 3: (L, C) Normalized cosine similarity of $I \otimes H_1$, A, and different sequence counts for B, calculated against H . A and B are both much closer to H than $I \otimes H_1$. (R) Average cosine similarity between A and B, grouped by linear layer. A and B are close, with pre-attention layers being closer.

H_O . By applying incoherence processing, we can bound the incoherences of H_O and H_I , which empirically translates to a lower trace bound.

Figure 3 L and C contain plots of the “normalized” cosine similarity of A, B, and $I \otimes H_1$ (LDLQ’s Hessian). Here, the normalized cosine similarity denotes $\frac{\langle H, H_O \otimes H_I \rangle}{\|H_O\| \|H_I\|}$, scaled so the largest data point is 1.0. This avoids computing $\|H\|$, which is unnecessary. The cosine similarities of A and B are both much higher than $I \otimes H_1$, with A being slightly lower than B. In certain data-limited cases, such as for layer 24 Down in Llama 3.1 8B Instruct, A has a higher cosine similarity than B. Here, the bias of A is less than the variance of B. Finally, Figure 3 R shows that A and B have high cosine similarities to each other, with the pre-attention score layers (Q, K) having higher similarity than the post-attention score layers. This correlates with our construction of A, which ignores sequence mixing. Indeed, across all desiderata, YAQA is provably better than LDLQ.

4 EXPERIMENTS

To test YAQA, we quantized Llama and Gemma models and evaluated both downstream performance (perplexity, zero-shot accuracy) and the KL divergence to the original model outputs. The KL considers the entire distribution over the output space, whereas perplexity and zero-shot accuracy only consider the mass of a single “ground truth” token (see Appendix). Since our goal is to produce a model as close to the original model as possible and almost all real-world use cases of LLMs involve sampling from the entire distribution, the KL is a more accurate indicator of how close two models are.

Baselines and Setup The focus of YAQA is on the Hessian estimate and rounding algorithm, so our main experiments perform PTQ without any additional finetuning. However, we include experiments with recovery finetuning to show that YAQA composes with finetuning. For YAQA-A, we use a context length of 8K, 20M tokens, and 3 full rounds of power iteration. For YAQA-B, we use a context length of 2K and 64K sequences.

In the following sections, we compare against LDLQ (Chee et al., 2023), GuidedQuant (Kim et al., 2025), DiscQuant (Chee et al., 2025), and Google’s QAT recipe (Team et al., 2025), which represent state-of-the-art algorithms that perform local adaptive rounding, end-to-end adaptive rounding, constrained gradient-based rounding, and QAT, respectively. Additional experiments and comparisons to CBQ (Ding et al., 2025) and PV-Tuning (Malinovskii et al., 2024) can be found in the Appendix. Of these, only LDLQ does not require computing gradients, and QAT requires significantly more data than the others. Regardless, YAQA achieves a lower KL than *all baselines* while achieving state of the art downstream performance.

4.1 SECOND ORDER QUANTIZATION ALGORITHMS

Table 1 compares YAQA against LDLQ and GuidedQuant, which respectively use local and global second order information during adaptive rounding. YAQA consistently outperforms both LDLQ and GuidedQuant in all metrics, with YAQA-B being better than YAQA-A as expected. In Section 3.2.3, we showed that LDLQ was provably worse than YAQA; indeed, this is reflected empirically. GuidedQuant uses a block diagonal approximation of the empirical Fisher and runs LDLQ on each block. Although GuidedQuant outperforms LDLQ and prior “end-to-end” methods like SqueezeLLM,

Table 1: Results with incoherence processing, the QTIP quantizer, and no finetuning. YAQA strongly outperforms LDLQ and GuidedQuant, two state-of-the-art local and global adaptive rounding methods. YAQA reduces the KL by a factor of $\approx 1/3$ over LDLQ. See Appendix for individual zeroshot results.

| ALGO. | BITS | $D_{KL} \downarrow$ | | $PPL \downarrow$ | | 0-SHOT \uparrow | | $D_{KL} \downarrow$ | | $PPL \downarrow$ | | 0-SHOT \uparrow | |
|---------------|------|---------------------|-------------|------------------|--------------|-------------------|---|---------------------|--------------|------------------|--------------|-------------------|--|
| | | W2 | C4 | W2 | C4 | Avg | | W2 | C4 | W2 | C4 | Avg | |
| 3.1 70B INST. | | | | | | | | | | | | 3.2 3B INST. | |
| BF16 | 16 | 0 | 3.52 | 6.46 | 67.67 | | | 0 | 9.58 | 10.62 | 63.79 | | |
| | 2 | 0.497 | 6.02 | 7.82 | 65.45 | | | 0.455 | 15.30 | 14.69 | 55.68 | | |
| | 3 | 0.138 | 4.26 | 6.74 | 67.58 | | | 0.085 | 10.69 | 11.44 | 62.46 | | |
| LDLQ | 4 | 0.045 | 3.74 | 6.54 | 67.58 | | | 0.021 | 9.78 | 10.79 | 63.70 | | |
| | 2 | 0.383 | 5.59 | 7.51 | 65.44 | | | 0.342 | 13.56 | 13.96 | 57.72 | | |
| | 3 | 0.111 | 4.10 | 6.68 | 67.33 | | | 0.070 | 10.48 | 11.19 | 63.48 | | |
| GUIDEDQUANT | 4 | 0.035 | 3.72 | 6.53 | 67.80 | | | 0.019 | 9.84 | 10.80 | 64.10 | | |
| | 2 | 0.378 | 5.56 | 7.51 | 65.92 | | | 0.333 | 13.75 | 13.56 | 58.29 | | |
| | 3 | 0.110 | 4.10 | 6.68 | 67.69 | | | 0.059 | 10.37 | 11.14 | 62.51 | | |
| YAQA-A | 4 | 0.036 | 3.73 | 6.52 | 67.50 | | | 0.015 | 9.78 | 10.76 | 63.28 | | |
| | 2 | 0.335 | 5.30 | 7.34 | 66.19 | | | 0.288 | 13.18 | 13.10 | 59.11 | | |
| | 3 | 0.094 | 4.01 | 6.64 | 67.24 | | | 0.047 | 10.15 | 11.09 | 62.74 | | |
| YAQA-B | 4 | 0.030 | 3.69 | 6.51 | 67.73 | | | 0.014 | 9.80 | 10.75 | 63.31 | | |
| 3.1 8B INST. | | | | | | | | | | | | 3.2 1B INST. | |
| BF16 | 16 | 0 | 6.50 | 8.02 | 69.82 | | 0 | 11.57 | 13.20 | 54.79 | | | |
| LDLQ | 2 | 0.356 | 9.39 | 10.70 | 62.51 | | | 0.527 | 19.86 | 19.66 | 49.60 | | |
| | 3 | 0.069 | 7.05 | 8.50 | 69.29 | | | 0.109 | 12.95 | 14.44 | 52.89 | | |
| | 4 | 0.019 | 6.63 | 8.15 | 69.41 | | | 0.032 | 12.05 | 13.63 | 53.47 | | |
| GUIDEDQUANT | 2 | 0.317 | 9.03 | 10.42 | 63.12 | | | 0.473 | 18.95 | 19.54 | 48.76 | | |
| | 3 | 0.062 | 6.98 | 8.44 | 68.53 | | | 0.095 | 12.82 | 14.33 | 53.48 | | |
| | 4 | 0.018 | 6.65 | 8.14 | 69.05 | | | 0.027 | 11.93 | 13.54 | 54.18 | | |
| YAQA-A | 2 | 0.284 | 8.79 | 10.09 | 64.06 | | | 0.371 | 17.22 | 17.64 | 50.02 | | |
| | 3 | 0.050 | 6.89 | 8.38 | 69.09 | | | 0.072 | 12.56 | 14.02 | 53.86 | | |
| | 4 | 0.015 | 6.62 | 8.13 | 69.62 | | | 0.021 | 11.83 | 13.44 | 54.17 | | |
| YAQA-B | 2 | 0.241 | 8.39 | 9.83 | 64.32 | | | 0.334 | 16.66 | 17.36 | 50.90 | | |
| | 3 | 0.044 | 6.85 | 8.34 | 69.31 | | | 0.065 | 12.51 | 13.97 | 53.41 | | |
| | 4 | 0.013 | 6.61 | 8.12 | 69.78 | | | 0.019 | 11.83 | 13.41 | 53.84 | | |

Table 2: Results with incoherence processing, the INT4 quantizer, and no finetuning for Llama 3.1 8B Instruct. YAQA is quantizer agnostic and works with standard datatypes such as INT4.

| ALGO. | $D_{KL} \downarrow$ | | $PPL \downarrow$ | | 0-SHOT ACC \uparrow | | | | | |
|-----------|---------------------|-------------|------------------|--------------|-----------------------|-------|-------|-------|-------|------|
| | W2 | C4 | W2 | C4 | Avg | ARCC | ARCE | BOOLQ | HSWAG | PiQA |
| BF16 | 0 | 6.50 | 8.02 | 69.82 | 51.37 | 78.03 | 82.05 | 57.74 | 79.92 | |
| LDLQ | 0.038 | 6.76 | 8.26 | 67.99 | 50.00 | 76.94 | 77.01 | 56.83 | 79.16 | |
| DISCQUANT | 0.061 | 6.83 | 8.37 | 67.68 | 50.34 | 77.44 | 74.12 | 56.55 | 79.92 | |
| YAQA-A | 0.028 | 6.71 | 8.21 | 69.11 | 50.68 | 78.11 | 79.65 | 57.13 | 79.98 | |
| YAQA-B | 0.029 | 6.72 | 8.23 | 68.92 | 49.49 | 77.31 | 81.01 | 56.98 | 79.82 | |

neither its Hessian or rounding algorithm come with easy-to-compute bounds on the end-to-end error. In contrast, YAQA both comes with theoretical guarantees and empirically outperforms GuidedQuant.

4.1.1 FIRST ORDER QUANTIZATION METHODS

Tables 2 and 3 compare YAQA with descent-style approaches. Since these methods require requantization or projection at every step, they are effectively limited to suboptimal scalar quantizers. In contrast, YAQA is a general rounding algorithm that can be used with any quantizer. Regardless, even when used with scalar quantizers, YAQA outperforms these methods. Table 2 compares YAQA to DiscQuant, which performs gradient descent on the KL in a localized subspace. Both YAQA and LDLQ outperform DiscQuant, showing that unlike YAQA, descent-based methods do not always outperform local adaptive rounding. Table 3 compares YAQA against Google’s QAT Gemma 3

Table 3: Results for Gemma 3 12B Inst. with INT4 *without finetuning*. Despite being trained on the original model’s outputs, the QAT model has a higher KL to the original model than YAQA.

| ALGO. | QUANT. TYPE | BITS | $D_{KL} \downarrow$ | PPL \downarrow | | | 0-SHOT ACC \uparrow | | | | |
|------------|-------------|------|---------------------|------------------|------|-------|-----------------------|-------|-------|-------|-------|
| | | | W2 | W2 | C4 | Avg | ARCC | ARCE | BOOLQ | HSWAG | PiQA |
| BF16 | NONE | 16 | 0 | 7.85 | 8.61 | 70.22 | 54.01 | 78.79 | 87.25 | 54.27 | 76.77 |
| GOOGLE QAT | QAT | 4.5 | 0.089 | 7.56 | 8.52 | 70.83 | 54.52 | 79.76 | 86.82 | 54.77 | 78.29 |
| YAQA-A | PTQ | 4 | 0.058 | 7.96 | 8.69 | 70.12 | 53.90 | 78.83 | 87.09 | 53.68 | 77.09 |
| YAQA-B | PTQ | 4 | 0.056 | 7.94 | 8.67 | 69.90 | 54.10 | 78.66 | 86.91 | 54.13 | 75.68 |

Table 4: Results with the QTIP quantizer, incoherence processing, and recovery finetuning. Although finetuning reduces the gap between YAQA and LDLQ, YAQA still achieves state-of-the-art results.

| ALGO. | BITS | $D_{KL} \downarrow$ | PPL \downarrow | | | 0-SHOT \uparrow | $D_{KL} \downarrow$ | PPL \downarrow | | | 0-SHOT \uparrow |
|------------------------|------|---------------------|------------------|-------------|--------------|-------------------|---------------------|------------------|-------------|--------------|-------------------|
| | | W2 | W2 | C4 | Avg | W2 | W2 | C4 | Avg | W2 | Avg |
| LLAMA 3.1 70B INSTRUCT | | | | | | | | | | | |
| BF16 | 16 | 0 | 3.52 | 6.46 | 67.67 | | 0 | 6.50 | 8.02 | 69.82 | |
| LDLQ | 2 | 0.302 | 5.01 | 7.16 | 66.11 | | 0.185 | 7.82 | 9.20 | 65.44 | |
| | 3 | 0.101 | 3.96 | 6.64 | 67.46 | | 0.048 | 6.80 | 8.31 | 68.42 | |
| | 4 | 0.036 | 3.71 | 6.54 | 67.64 | | 0.016 | 6.61 | 8.13 | 69.47 | |
| | 2 | 0.279 | 4.92 | 7.10 | 66.26 | | 0.163 | 7.63 | 9.06 | 67.54 | |
| YAQA-A | 3 | 0.098 | 3.88 | 6.63 | 66.94 | | 0.042 | 6.78 | 8.28 | 69.23 | |
| | 4 | 0.032 | 3.68 | 6.52 | 67.59 | | 0.014 | 6.58 | 8.10 | 69.50 | |
| | 2 | 0.266 | 4.82 | 7.07 | 66.99 | | 0.147 | 7.60 | 8.96 | 66.38 | |
| YAQA-B | 3 | 0.091 | 3.87 | 6.61 | 67.42 | | 0.038 | 6.74 | 8.27 | 68.88 | |
| | 4 | 0.029 | 3.67 | 6.52 | 67.69 | | 0.012 | 6.56 | 8.11 | 70.12 | |

12B Instruct (Team et al., 2025). We estimate the QAT process took $100\times$ more data than YAQA. Although the QAT model somehow outperforms the original model in downstream tasks, *even without finetuning*, YAQA models have a lower KL divergence to the original model. YAQA also maintains a smaller gap in downstream performance, suggesting that QAT actually produces a considerably different model and YAQA better preserves the original model.

4.2 FINETUNING

Recent PTQ works have included a “recovery finetuning” step that adjusts unquantized parameters *before quantization* to compensate for the effect of *already-quantized layers* (Tseng et al., 2024a;b; Egiazarian et al., 2024; Malinovskii et al., 2024). This effectively includes cross layer information, which raises the question: how much overlap is there between finetuning and YAQA? Table 4 shows an experiment with QuIP#’s recovery finetuning algorithm and the setup in Table 1. For both models, recovery finetuning reduces the gap between LDLQ and YAQA. However, YAQA still reduces the KL by $\approx 10\text{-}20\%$ over LDLQ and maintains a large gap in downstream tasks, indicating that YAQA uses global information that is not available during recovery finetuning. Finally, the LDLQ results in this table correspond to the results in the state-of-the-art QTIP paper, so YAQA’s results Table 4 set a new state of the art across all PTQ methods and quantizers.

5 CONCLUSION

In this work, we present YAQA, a new rounding algorithm that generalizes state-of-the-art local layerwise quantization methods to minimize the end-to-end error. YAQA introduces a series of theoretical results that give, for the first time, end-to-end error bounds for quantization algorithms. These results admit a natural Kronecker-factored Hessian structure for use with adaptive rounding algorithms, as well as corresponding near-optimal Hessian sketches. YAQA is provably better than GPTQ/LDLQ and empirically reduces the KL by $\approx 30\%$ over these methods. Even further, YAQA achieves a lower KL than QAT and sets a new empirical state-of-the-art in downstream tasks among PTQ methods, all while adding no inference overhead.

ETHICS AND REPRODUCIBILITY STATEMENT

This paper presents work whose goal is to advance the field of Machine Learning. There are many potential societal consequences of our work, none which we feel must be specifically highlighted here. Details to reproduce our experiments are in the main body and Appendix, and our code will be released at a later date.

REFERENCES

Jerry Chee, Yaohui Cai, Volodymyr Kuleshov, and Christopher De Sa. QuIP: 2-bit quantization of large language models with guarantees. In *Thirty-seventh Conference on Neural Information Processing Systems*, 2023. URL <https://openreview.net/forum?id=xrk9g5vcXR>.

Jerry Chee, Arturs Backurs, Rainie Heck, Li Zhang, Janardhan Kulkarni, Thomas Rothvoss, and Sivakanth Gopi. Discquant: A quantization method for neural networks inspired by discrepancy theory, 2025. URL <https://arxiv.org/abs/2501.06417>.

Together Computer. Redpajama: An open source recipe to reproduce llama training dataset, 2023. URL <https://github.com/togethercomputer/RedPajama-Data>.

Christopher De Sa, Albert Gu, Rohan Puttagunta, Christopher Ré, and Atri Rudra. A two pronged progress in structured dense matrix multiplication, 2017. URL <https://arxiv.org/abs/1611.01569>.

Xin Ding, Xiaoyu Liu, Zhijun Tu, Yun Zhang, Wei Li, Jie Hu, Hanting Chen, Yehui Tang, Zhiwei Xiong, Baoqun Yin, and Yunhe Wang. CBQ: Cross-block quantization for large language models. In *The Thirteenth International Conference on Learning Representations*, 2025. URL <https://openreview.net/forum?id=eW4yh6HKz4>.

Vage Egiazarian, Andrei Panferov, Denis Kuznedelev, Elias Frantar, Artem Babenko, and Dan Alistarh. Extreme compression of large language models via additive quantization, 2024.

Elias Frantar, Saleh Ashkboos, Torsten Hoefer, and Dan Alistarh. OPTQ: Accurate quantization for generative pre-trained transformers. In *The Eleventh International Conference on Learning Representations*, 2023. URL <https://openreview.net/forum?id=tcbBPnfwxs>.

Thomas George, César Laurent, Xavier Bouthillier, Nicolas Ballas, and Pascal Vincent. Fast approximate natural gradient descent in a kronecker factored eigenbasis. In S. Bengio, H. Wallach, H. Larochelle, K. Grauman, N. Cesa-Bianchi, and R. Garnett (eds.), *Advances in Neural Information Processing Systems*, volume 31. Curran Associates, Inc., 2018. URL https://proceedings.neurips.cc/paper_files/paper/2018/file/48000647b315f6f00f913caa757a70b3-Paper.pdf.

Christian Gourieroux and Alain Monfort. *Statistics and Econometric Models*. Number 9780521471626 in Cambridge Books. Cambridge University Press, December 1995. URL <https://ideas.repec.org/b/cup/cbooks/9780521471626.html>.

Vineet Gupta, Tomer Koren, and Yoram Singer. Shampoo: Preconditioned stochastic tensor optimization. In Jennifer Dy and Andreas Krause (eds.), *Proceedings of the 35th International Conference on Machine Learning*, volume 80 of *Proceedings of Machine Learning Research*, pp. 1842–1850. PMLR, 10–15 Jul 2018. URL <https://proceedings.mlr.press/v80/gupta18a.html>.

Babak Hassibi, David Stork, and Gregory Wolff. Optimal brain surgeon: Extensions and performance comparisons. In J. Cowan, G. Tesauro, and J. Alspector (eds.), *Advances in Neural Information Processing Systems*, volume 6. Morgan-Kaufmann, 1993. URL https://proceedings.neurips.cc/paper_files/paper/1993/file/b056eb1587586b71e2da9acfe4fb19e-Paper.pdf.

Jordan Hoffmann, Sebastian Borgeaud, Arthur Mensch, Elena Buchatskaya, Trevor Cai, Eliza Rutherford, Diego de Las Casas, Lisa Anne Hendricks, Johannes Welbl, Aidan Clark, Tom Hennigan, Eric Noland, Katie Millican, George van den Driessche, Bogdan Damoc, Aurelia Guy,

Simon Osindero, Karen Simonyan, Erich Elsen, Jack W. Rae, Oriol Vinyals, and Laurent Sifre. Training compute-optimal large language models, 2022. URL <https://arxiv.org/abs/2203.15556>.

Jinuk Kim, Marwa El Halabi, Wonpyo Park, Clemens JS Schaefer, Deokjae Lee, Yeonhong Park, Jae W. Lee, and Hyun Oh Song. Guidedquant: Large language model quantization via exploiting end loss guidance. In *Forty-second International Conference on Machine Learning*, 2025. URL <https://openreview.net/forum?id=ZawsPj1IGu>.

Sehoon Kim, Coleman Hooper, Amir Gholami, Zhen Dong, Xiuyu Li, Sheng Shen, Michael Mahoney, and Kurt Keutzer. Squeezellm: Dense-and-sparse quantization. *arXiv*, 2023.

Frederik Kunstner, Lukas Balles, and Philipp Hennig. Limitations of the empirical fisher approximation for natural gradient descent, 2020. URL <https://arxiv.org/abs/1905.12558>.

Ji Lin, Jiaming Tang, Haotian Tang, Shang Yang, Xingyu Dang, Chuang Gan, and Song Han. Awq: Activation-aware weight quantization for llm compression and acceleration, 2023.

Charles F.Van Loan. The ubiquitous kronecker product. *Journal of Computational and Applied Mathematics*, 123(1):85–100, 2000. ISSN 0377-0427. doi: [https://doi.org/10.1016/S0377-0427\(00\)00393-9](https://doi.org/10.1016/S0377-0427(00)00393-9). URL <https://www.sciencedirect.com/science/article/pii/S0377042700003939>. Numerical Analysis 2000. Vol. III: Linear Algebra.

Vladimir Malinovskii, Denis Mazur, Ivan Ilin, Denis Kuznedelev, Konstantin Pavlovich Burlachenko, Kai Yi, Dan Alistarh, and Peter Richtárik. PV-tuning: Beyond straight-through estimation for extreme LLM compression. In *The Thirty-eighth Annual Conference on Neural Information Processing Systems*, 2024. URL <https://openreview.net/forum?id=YvA8UF0I37>.

James Martens and Roger Grosse. Optimizing neural networks with kronecker-factored approximate curvature. In Francis Bach and David Blei (eds.), *Proceedings of the 32nd International Conference on Machine Learning*, volume 37 of *Proceedings of Machine Learning Research*, pp. 2408–2417, Lille, France, 07–09 Jul 2015. PMLR. URL <https://proceedings.mlr.press/v37/martens15.html>.

Depen Morwani, Itai Shapira, Nikhil Vyas, eran malach, Sham M. Kakade, and Lucas Janson. A new perspective on shampoo’s preconditioner. In *The Thirteenth International Conference on Learning Representations*, 2025. URL <https://openreview.net/forum?id=c6zI3Cp8c6>.

Markus Nagel, Rana Ali Amjad, Mart Van Baalen, Christos Louizos, and Tijmen Blankevoort. Up or down? Adaptive rounding for post-training quantization. In Hal Daumé III and Aarti Singh (eds.), *Proceedings of the 37th International Conference on Machine Learning*, volume 119 of *Proceedings of Machine Learning Research*, pp. 7197–7206. PMLR, 13–18 Jul 2020. URL <https://proceedings.mlr.press/v119/nagel20a.html>.

Markus Nagel, Marios Fournarakis, Yelysei Bondarenko, and Tijmen Blankevoort. Overcoming oscillations in quantization-aware training. In Kamalika Chaudhuri, Stefanie Jegelka, Le Song, Csaba Szepesvari, Gang Niu, and Sivan Sabato (eds.), *Proceedings of the 39th International Conference on Machine Learning*, volume 162 of *Proceedings of Machine Learning Research*, pp. 16318–16330. PMLR, 17–23 Jul 2022. URL <https://proceedings.mlr.press/v162/nagel22a.html>.

Neil Sloane. Hadamard Matrices — neilsloane.com. <http://neilsloane.com/hadamard/>. [Accessed 02-02-2024].

Gemma Team, Aishwarya Kamath, Johan Ferret, Shreya Pathak, Nino Vieillard, Ramona Merhej, Sarah Perrin, Tatiana Matejovicova, Alexandre Ramé, Morgane Rivière, Louis Rouillard, Thomas Mesnard, Geoffrey Cideron, Jean bastien Grill, Sabela Ramos, Edouard Yvinec, Michelle Casbon, Etienne Pot, Ivo Penchev, Gaël Liu, Francesco Visin, Kathleen Kenealy, Lucas Beyer, Xiaohai Zhai, Anton Tsitsulin, Robert Busa-Fekete, Alex Feng, Noveen Sachdeva, Benjamin Coleman, Yi Gao, Basil Mustafa, Iain Barr, Emilio Parisotto, David Tian, Matan Eyal, Colin Cherry, Jan-Thorsten Peter, Danila Sinopalnikov, Surya Bhupatiraju, Rishabh Agarwal, Mehran Kazemi, Dan Malkin, Ravin Kumar, David Vilar, Idan Brusilovsky, Jiaming Luo, Andreas Steiner, Abe

Friesen, Abhanshu Sharma, Abheesht Sharma, Adi Mayrav Gilady, Adrian Goedeckemeyer, Alaa Saade, Alex Feng, Alexander Kolesnikov, Alexei Bendebury, Alvin Abdagic, Amit Vadi, András György, André Susano Pinto, Anil Das, Ankur Bapna, Antoine Miech, Antoine Yang, Antonia Paterson, Ashish Shenoy, Ayan Chakrabarti, Bilal Piot, Bo Wu, Bobak Shahriari, Bryce Petrini, Charlie Chen, Charline Le Lan, Christopher A. Choquette-Choo, CJ Carey, Cormac Brick, Daniel Deutsch, Danielle Eisenbud, Dee Cattle, Derek Cheng, Dimitris Paparas, Divyashree Shivakumar Sreepathihalli, Doug Reid, Dustin Tran, Dustin Zelle, Eric Noland, Erwin Huizenga, Eugene Kharitonov, Frederick Liu, Gagik Amirkhanyan, Glenn Cameron, Hadi Hashemi, Hanna Klimczak-Plucińska, Harman Singh, Harsh Mehta, Harshal Tushar Lehri, Hussein Hazimeh, Ian Ballantyne, Idan Szpektor, Ivan Nardini, Jean Pouget-Abadie, Jetha Chan, Joe Stanton, John Wieting, Jonathan Lai, Jordi Orbay, Joseph Fernandez, Josh Newlan, Ju yeong Ji, Jyotiinder Singh, Kat Black, Kathy Yu, Kevin Hui, Kiran Vodrahalli, Klaus Greff, Linhai Qiu, Marcella Valentine, Marina Coelho, Marvin Ritter, Matt Hoffman, Matthew Watson, Mayank Chaturvedi, Michael Moynihan, Min Ma, Nabila Babar, Natasha Noy, Nathan Byrd, Nick Roy, Nikola Momchev, Nilay Chauhan, Noveen Sachdeva, Oskar Bunyan, Pankil Botarda, Paul Caron, Paul Kishan Rubenstein, Phil Culliton, Philipp Schmid, Pier Giuseppe Sessa, Pingmei Xu, Piotr Stanczyk, Pouya Tafti, Rakesh Shivanna, Renjie Wu, Renke Pan, Reza Rokni, Rob Willoughby, Rohith Vallu, Ryan Mullins, Sammy Jerome, Sara Smoot, Sertan Girgin, Shariq Iqbal, Shashir Reddy, Shruti Sheth, Siim Pöder, Sijal Bhatnagar, Sindhu Raguram Panyam, Sivan Eiger, Susan Zhang, Tianqi Liu, Trevor Yacovone, Tyler Liechty, Uday Kalra, Utku Evcı, Vedant Misra, Vincent Roseberry, Vlad Feinberg, Vlad Kolesnikov, Woohyun Han, Woosuk Kwon, Xi Chen, Yinlam Chow, Yuvein Zhu, Zichuan Wei, Zoltan Egyed, Victor Cotruta, Minh Giang, Phoebe Kirk, Anand Rao, Kat Black, Nabila Babar, Jessica Lo, Erica Moreira, Luiz Gustavo Martins, Omar Sanseviero, Lucas Gonzalez, Zach Gleicher, Tris Warkentin, Vahab Mirrokni, Evan Senter, Eli Collins, Joelle Barral, Zoubin Ghahramani, Raia Hadsell, Yossi Matias, D. Sculley, Slav Petrov, Noah Fiedel, Noam Shazeer, Oriol Vinyals, Jeff Dean, Demis Hassabis, Koray Kavukcuoglu, Clement Farabet, Elena Buchatskaya, Jean-Baptiste Alayrac, Rohan Anil, Dmitry Lepikhin, Sebastian Borgeaud, Olivier Bachem, Armand Joulin, Alek Andreev, Cassidy Hardin, Robert Dadashi, and Léonard Hussenot. Gemma 3 technical report, 2025. URL <https://arxiv.org/abs/2503.19786>.

Albert Tseng, Jerry Chee, Qingyao Sun, Volodymyr Kuleshov, and Christopher De Sa. Quip#: Even better ILM quantization with hadamard incoherence and lattice codebooks, 2024a.

Albert Tseng, Qingyao Sun, David Hou, and Christopher De Sa. QTIP: Quantization with trellises and incoherence processing. In *The Thirty-eighth Annual Conference on Neural Information Processing Systems*, 2024b. URL <https://openreview.net/forum?id=7sdkLVuYCU>.

Albert Tseng, Tao Yu, and Youngsuk Park. Training LLMs with MXFP4. In *The 28th International Conference on Artificial Intelligence and Statistics*, 2025. URL <https://openreview.net/forum?id=a8z5Q0WSPL>.

Nikhil Vyas, Depen Morwani, Rosie Zhao, Itai Shapira, David Brandfonbrener, Lucas Janson, and Sham M. Kakade. SOAP: Improving and stabilizing shampoo using adam for language modeling. In *The Thirteenth International Conference on Learning Representations*, 2025. URL <https://openreview.net/forum?id=IDxZhXrpNf>.

A APPENDIX

A.1 EXPERIMENTAL SETUP AND IMPLEMENTATION DETAILS

All Hessians were collected using the RedPajama v1 dataset Computer (2023). We use Hadamard matrices from Neil Sloane’s website for the “base Hadamard matrix” in incoherence processing as described in Section A.5 Sloane. We use the OPTQ “Wikitext2” and “C4” dataset splits for KL divergence and perplexity calculation Frantar et al. (2023). We use a sequence length of 8192 for all KL divergence and perplexity evaluations. We evaluate all zero-shot results with the chat template applied. For finetuning experiments, we use the same setup as QTIP except that we normalize the activation error due to numerical instability from the default Adam $\epsilon = 10^{-8}$. For all Llama 3.1 70B Instruct experiments, we do not quantize the `0_v` layer. The Gemma QAT comparison was run with the `google/gemma-3-12b-it-qat-q4_0-gguf` model on Huggingface, which was dequantized with the `4.52.0.dev0` nightly version of Transformers.

A.2 HESSIAN SKETCH MEMORY AND COMPUTE REQUIREMENTS

YQAQ requires storing $O(n^2)$ memory for H_I and $O(m^2)$ memory for H_O . In practice, we only need to store the lower triangular parts of H_I and H_O since they are symmetric. LDLQ and other layerwise activation methods only need to store H_I , so YQAQ requires roughly double the storage for the Hessians. We found that computing and storing the Hessians in FP32 was sufficient to maintain numerical stability and positive-definiteness with a small regularization factor on the diagonal ($\approx 10^{-4} \text{tr}(H)/n$), but using TF32 for computations was not. The computational cost of computing Hessians with Sketch B is $O(btmn + bn^2m + bm^2n)$ on top of the cost of a forward pass and backprop, where b is the number of sequences and t is the average number of tokens per sequence. The computational cost of computing Hessians with Sketch A is $O(pbt(n^2 + m^2))$, again on top of a forward pass and backward pass, where p is the number of steps of power iteration. Since we must use a larger b for Sketch B than Sketch A to get acceptable variance, Sketch B is empirically slower than Sketch A.

A.3 GUIDEDQUANT AS LDLQ

In GuidedQuant, each of g groups of output channels in W^* shares an input Hessian for LDLQ. This corresponds to a block-diagonal Hessian approximation, where there are $g \leq m$ unique $n \times n$ blocks. Since the L part of the LDL decomposition of a matrix is block lower unit triangular, observe that the SND of this approximation is simply the largest SND of any given block. This is n , which matches an optimal implementation of GuidedQuant where LDLQ is run in parallel across groups. However, observe that even though the number of serial steps is n , the number of FLOPs is increased by a factor of g , which means that GuidedQuant is still more expensive than regular LDLQ when $g > 1$.

A.4 KL DIVERGENCE VS. PERPLEXITY

While the full model KL divergence and perplexity are conceptually related, they measure two fundamentally different quantities. The KL measures the difference between two distributions and is defined over the full support of the distributions as $D_{\text{KL}}(p\|q) = \sum_{x \in \mathcal{X}} p(x) \log \frac{p(x)}{q(x)}$. The perplexity measures the mass on a “ground truth” target τ in single probability distribution p : $1/p(\tau)$. As such, two models can have very similar perplexities but be completely different from each other. For example, Llama 1 7B has a Wikitext 2 perplexity of 5.68 and Llama 2 7B has a perplexity of 5.47, but were pretrained from scratch separately. Indeed, their KL divergence is 0.197, which is much higher than what the difference in perplexity would suggest ($\log \left(\frac{5.68}{5.47} \right) = 0.038$)

A.5 INCOHERENCE PROCESSING WITH THE RANDOM HADAMARD TRANSFORM

Although we describe incoherence processing for Hessians in the main body, incoherence processing also modifies the weights. The full definition of incoherence, including *weight incoherence*, is as follows:

Definition 3 (Chee et al. (2023)). A Hessian $H \in \mathbb{R}^{n \times n}$ is μ -incoherent if its eigendecomposition $H = Q\Lambda Q^T$ has $\max_{i,j} |Q_{ij}| = \max_{i,j} |e_i^T Q e_j| \leq \mu/\sqrt{n}$. A weight matrix $W \in \mathbb{R}^{m \times n}$ is μ -incoherent if $\max_{i,j} |W_{ij}| = \max_{i,j} |e_i^T W e_j| \leq \mu \|W\|_F/\sqrt{mn}$.

Incoherence processing with the RHT applies a Random Hadamard Transformation on W and H . Let H be a Hadamard matrix, defined as follows:

$$H_1 = [1] \quad H_n = \frac{1}{\sqrt{2}} \begin{bmatrix} H_{n-1} & H_{n-1} \\ H_{n-1} & -H_{n-1} \end{bmatrix} \quad (11)$$

Then, the RHT performs $x \leftarrow H_{\log_2 n} S x$, where S is a random sign vector $\in \{\pm 1\}^n$, $x \in \mathbb{R}^n$, and n is a power of 2. For non power-of-2 n , we follow QuIP# and use a fixed “small” Hadamard matrix as a base instead of H_1 . Full proofs for bounds on the behavior of the RHT can be found in QuIP#.

A.6 YAQA ROUNDING ALGORITHM

The YAQA rounding algorithm can be written as a fixed point iteration (Algorithm 1). It can also be implemented iteratively (Python code), which is faster for slower quantizers than the fixed point iteration implementation above.

Algorithm 1 YAQA Rounding Algorithm Fixed Point Iteration

Require: Weight matrix $W \in \mathbb{R}^{m \times n}$, p.d. $H_O \in \mathbb{R}^{m \times m}$, p.d. $H_I \in \mathbb{R}^{n \times n}$, quantizer \mathcal{Q} , quantizer block sizes $g_x \in \mathbb{Z}^+ | m, g_y \in \mathbb{Z}^+ | n$.

- 1: $L_O, D_O \leftarrow \text{BlockLDL}(H_O, g_x)$
- 2: $L_I, D_I \leftarrow \text{BlockLDL}(H_I, g_y)$
- 3: $\hat{W} \leftarrow \mathcal{Q}(W)$
- 4: $\text{converged} \leftarrow \text{false}$
- 5: $\hat{W}^* \leftarrow \hat{W}$
- 6: **while** not converged **do**
- 7: $\Delta W \leftarrow W - \hat{W}$
- 8: $\hat{W} = \mathcal{Q}(W + L_O^T \Delta W L_I + L_O^T \Delta W + \Delta W L_I)$
- 9: $\text{converged} \leftarrow (\hat{W} == \hat{W}^*)$
- 10: $\hat{W}^* \leftarrow \hat{W}$
- 11: **end while**
- 12: **return** Quantized \hat{W} .

```
def YAQA_iterative(W, Lin, Lout, td_x, td_y, cb):
    m, n = W.shape
    hatW = torch.zeros_like(W)
    Qidxs = torch.zeros(m, n, dtype=cb.idx_dtype, device=W.device)
    assert m % td_x == 0 and n % td_y == 0
    starts = [*[(m//td_x-i-1, n//td_y-1) for i in range(m//td_x)], *[0, n//td_y-i-1) for i in range(n//td_y)]]

    for i in tqdm(range(m//td_x + n//td_y)):
        target = []
        target_idx = []
        start = starts[i]
        jmax = max(start[0], start[1])
        jm, jn = start
        while 0 <= jm < m//td_x and 0 <= jn < n//td_y:
            thing = W[jm*td_x:(jm+1)*td_x, jn*td_y:(jn+1)*td_y] + (Lout[jm*td_x:, jm*td_x:(jm+1)*td_x].T @ (W[jm*td_x:, jn*td_y:] - hatW[jm*td_x:, jn*td_y:]) @ Lin[jn*td_y:, jn*td_y:(jn+1)*td_y] + Lout[jm*td_x:, jm*td_x:(jm+1)*td_x].T @ (W[jm*td_x:, jn*td_y:(jn+1)*td_y] - hatW[jm*td_x:, jn*td_y:(jn+1)*td_y]) + (W[jm*td_x:(jm+1)*td_x, jn*td_y:] - hatW[jm*td_x:(jm+1)*td_x, jn*td_y:(jn+1)*td_y]) @ Lin[jn*td_y:, jn*td_y:(jn+1)*td_y])
            target.append(thing)
            target_idx.append((jm, jn))
            jm += 1
            jn -= 1

        target = torch.stack(target, dim=0).reshape(-1, td_x * td_y)
        qtarget, target_idx = cb.quantize(target)
        qtarget = qtarget.reshape(-1, td_x, td_y)
```

```

target_idx = target_idx.reshape(-1, td_x, td_y)

for j in range(len(target_idx)):
    jm, jn = target_idx[j]
    hatW[jm*td_x:(jm+1)*td_x, jn*td_y:(jn+1)*td_y] = qtarget[j]
    Qidxs[jm*td_x:(jm+1)*td_x, jn*td_y:(jn+1)*td_y] = target_idx[j]

return hatW, Qidxs

```

A.7 PROOFS

Lemma 1. *Equation 3 converges after at most $\text{snd}(L)$ steps.*

Proof. Consider the binary matrix B with the same support as $L - I$. This forms an adjacency matrix for the dependency graph of LDLQ , where $B_{i,j} = 1$ iff weight i is rounded with feedback from weight j . Since B has degree $k = \text{snd}(L)$, the DAG corresponding to the dependency graph has depth equal to k . Each step of LDLQ corresponds to advancing one level in the dependency DAG, so LDLQ converges in k steps. \square

Lemma 2. *Let L_1, L_2 be unit triangular matrices. Then $\text{snd}(L_1 \otimes L_2) = \text{snd}(L_1) + \text{snd}(L_2)$.*

Proof. Suppose that $N_1^{k_1} = (L_1 - I)^{k_1} = 0$ and similarly for N_2 and k_2 . Then, if $k = k_1 + k_2 - 1$,

$$(L_1 \otimes L_2 - I)^k = ((L_1 - I) \otimes (L_2 - I) + (L_1 - I) \otimes I + I \otimes (L_2 - I))^k \quad (12)$$

$$= (N_1 \otimes N_2 + N_1 \otimes I + I \otimes N_2)^k \quad (13)$$

$$= \sum_{i,j} \binom{k}{i,j} (N_1 \otimes N_2)^{k-i-j} \cdot (N_1 \otimes I)^i \cdot (I \otimes N_2)^j \quad (14)$$

$$= \sum_{i,j} \binom{k}{i,j} (N_1^{k-j} \otimes N_2^{k-i}), \quad (15)$$

where we can apply the multinomial theorem here to this matrix power because all these matrices ($N_1 \otimes N_2$, $N_1 \otimes I$, and $I \otimes N_2$) commute. But since this sum goes over $i + j \leq k$, it must be that $(k-j) + (k-i) = 2k - i - j \geq k = k_1 + k_2 - 1$. But this means that either $k-j \geq k_1$, or $k-i \geq k_2$ (since otherwise $k-j \leq k_1 - 1$ and $k-i \leq k_2 - 1$ and summing yields a contradiction). So then either N_1^{k-j} or N_2^{k-i} must be zero in each of these terms, and so we get $(L_1 \otimes L_2 - I)^k = 0$. \square

Theorem 2. *Let $H_O \in \mathbb{R}^{m \times m}$ and $H_I \in \mathbb{R}^{n \times n}$ be two positive definite matrices and let \mathcal{Q} perform nearest or stochastic rounding independently on blocks of $g_x \times g_y$ with $\mathbb{E}[(\mathcal{Q}(\text{vec}(x)) - \text{vec}(x))(\mathcal{Q}(\text{vec}(x)) - \text{vec}(x))^T] \preceq \sigma^2 I$. Furthermore, let W be the output of Equation 5 with L_O and L_I from the g_x and g_y -block LDL decompositions of H_O and H_I , respectively. Then,*

$$\Delta W (H_O \otimes H_I) \Delta W^T \leq \text{tr}(D_I) \text{tr}(D_O) g_x g_y \sigma^2 \leq \frac{g_x g_y \mu_I^2 \mu_O^2}{mn} \text{tr}(H_I^{1/2})^2 \text{tr}(H_O^{1/2})^2 \sigma^2$$

where $\Delta W = W^* - W$ and μ_O, μ_I are the incoherences of H_O, H_I (Definition 3).

Proof. Let

$$\eta = W^* + L_O^T \Delta W L_I + L_O^T \Delta W + \Delta W L_I - W \quad (16)$$

$$= (L_O + I)^T \Delta W (L_I + I) \quad (17)$$

Then,

$$\Delta W (H_O \otimes H_I) \Delta W^T = \text{tr}(\Delta W H_I \Delta W^T H_O) \quad (18)$$

$$= \text{tr}(\Delta W (L_I + I) D_I (L_I + I)^T \Delta W^T (L_O + I) H_O (L_O + I)^T) \quad (19)$$

$$= \text{tr}(\eta D_I \eta^T D_O) = \text{tr}(\eta^T \eta (D_O \otimes D_I)) \quad (20)$$

Since

$$\eta = W^* + L_O^T \Delta W L_I + L_O^T \Delta W + \Delta W L_I - W \quad (21)$$

$$= W^* + L_O^T \Delta W L_I + L_O^T \Delta W + \Delta W L_I - \mathcal{Q}(W^* + L_O^T \Delta W L_I + L_O^T \Delta W + \Delta W L_I) \quad (22)$$

$$= \star - Q(\star) \quad (23)$$

and \mathcal{Q} operates independently on $g_x \times g_y$ -sized blocks, we have that $\text{tr}(\eta^T \eta (D_O \otimes D_I)) \leq g_x g_y \sigma^2 \text{tr}(D_O \otimes D_I) = g_x g_y \sigma^2 \text{tr}(D_O) \text{tr}(D_I)$. From Chee et al. (2023), we have that

$$\text{tr}(D) \leq \frac{\mu}{k} \text{tr}(H^{1/2})^2 \quad (24)$$

for arbitrary p.d. $H \in \mathbb{R}^{k \times k}$, so

$$\text{tr}(D_O) \text{tr}(D_I) g_x g_y \sigma^2 \leq \frac{g_x g_y \mu_I^2 \mu_O^2}{mn} \text{tr}(H_I^{1/2})^2 \text{tr}(H_O^{1/2})^2 \sigma^2 \quad (25)$$

□

Theorem 3. Let $H_O \in \mathbb{R}^{m \times m}$ and $H_I \in \mathbb{R}^{n \times n}$ be two positive definite matrices and let \mathcal{Q} perform nearest or stochastic rounding with $\mathbb{E}[(\mathcal{Q}(x) - x)^2] \leq \sigma^2$. Furthermore, let W be the output of Equation 5 with L_O and L_I from the LDL decompositions of H_O and H_I , respectively. Then,

$$\Delta W (H_O \otimes H_I) \Delta W^T \leq \text{tr}(D_I) \text{tr}(D_O) \sigma^2 \leq \frac{\mu_I^2 \mu_O^2}{mn} \text{tr}(H_I^{1/2})^2 \text{tr}(H_O^{1/2})^2 \sigma^2$$

where $\Delta W = W^* - W$ and μ_O, μ_I are the incoherences of H_O, H_I (Definition 3).

Proof. This follows from setting $g_x = g_y = 1$ in Theorem 2. □

Lemma 3. Let $A, B \in \mathbb{R}^{n \times n}$ be positive definite matrices and $x \in \mathbb{R}^n$ be a vector. Then, $\left| x^T \frac{A}{\|A\|} x - x^T \frac{B}{\|B\|} x \right| \leq \|x\|_F^2 \sqrt{2 - 2c}$ where $\frac{\langle A, B \rangle}{\|A\| \|B\|} = c$.

Proof.

$$\left| x^T \frac{A}{\|A\|} x - x^T \frac{B}{\|B\|} x \right| = \left| x^T \left(\frac{A}{\|A\|} - \frac{B}{\|B\|} \right) x \right| \quad (26)$$

$$\leq \left\| \frac{A}{\|A\|} - \frac{B}{\|B\|} \right\|_F \|x\|_F^2 \quad (27)$$

$$\leq \|x\|_F^2 \sqrt{2 - 2c} \quad (28)$$

□

Theorem 1. Let $H \in \mathbb{R}^{mn \times mn} = \nabla^2 \mathcal{L}(W^*)$ be the Hessian of a linear layer W with respect to the KL to the original model outputs, $H_O \in \mathbb{R}^{m \times m}$ and $H_I \in \mathbb{R}^{n \times n}$ be two p.d. matrices, and \mathcal{Q} perform nearest or stoch. rounding with $\mathbb{E}[(\mathcal{Q}(x) - x)^2] \leq \sigma^2$. Furthermore, let W be the output of Equation 5 with L'_O, L'_I from the LDL decompositions of H_O, H_I , respectively. Then,

$$\text{vec}(\Delta) H \text{vec}(\Delta)^T \leq \|H\|_F \left(\|\Delta\|_F^2 \sqrt{2 - 2c} + \frac{\mu_I^2 \mu_O^2}{mn \|H_I\|_F \|H_O\|_F} \text{tr}(H_I^{1/2})^2 \text{tr}(H_O^{1/2})^2 \sigma^2 \right)$$

where $c = \frac{\langle H, H_O \otimes H_I \rangle}{\|H\|_F \|H_O\|_F \|H_I\|_F}$ is the cosine similarity between H and $H_O \otimes H_I$.

Proof. From Lemma 3, we have that

$$\left| \frac{\Delta W H \Delta W^T}{\|H\|} - \frac{\Delta W (H_O \otimes H_I) \Delta W^T}{\|H_O\| \|H_I\|} \right| \leq \|\Delta W\|_F^2 \sqrt{2 - 2c}. \quad (29)$$

Then,

$$\Delta W H \Delta W^T \leq \|H\| \left(\|\Delta W\|_F^2 \sqrt{2 - 2c} + \frac{\Delta W (H_O \otimes H_I) \Delta W^T}{\|H_O\| \|H_I\|} \right) \quad (30)$$

$$\Delta W H \Delta W^T \leq \|H\| \left(\|\Delta W\|_F^2 \sqrt{2 - 2c} + \frac{\mu_I^2 \mu_O^2}{mn \|H_I\| \|H_O\|} \text{tr}(H_I^{1/2})^2 \text{tr}(H_O^{1/2})^2 \sigma^2 \right). \quad (31)$$

□

A.8 MODIFIED PYTORCH BACKWARD PASS TO COMPUTE SKETCH A

```

class LinearNoBias(torch.autograd.Function):
    @staticmethod
    @torch.amp.custom_fwd(device_type='cuda')
    def forward(ctx, input, weight, mode, parent_class):
        ctx.save_for_backward(input, weight)
        ctx.mode = mode
        ctx.parent_class = parent_class

        return input @ weight.T

    @staticmethod
    @torch.amp.custom_bwd(device_type='cuda')
    def backward(ctx, grad_output):
        it, reset, div = ctx.mode
        is_buffer = local_rank == ctx.parent_class.buffer_dev

        input, weight = ctx.saved_tensors
        ws = weight.shape
        grad_input = grad_output @ weight
        del weight

        if ctx.parent_class.collect_hess:
            grad_output = grad_output.reshape(-1, grad_output.shape[-1])
            input = input.reshape(-1, input.shape[-1])
            op_dtype = ctx.parent_class.op_dtype
            with torch.amp.autocast('cuda', enabled=False):
                grad_output = grad_output.float()
                input = input.float()
                bs = input.shape[0]
            if it == 0:
                del grad_output
                if reset and is_buffer:
                    ctx.parent_class.hin.mul_(0)

            in_hess = sym_to_flat(input.T @ input) / ctx.parent_class.scale
            del input
            torch.distributed.reduce(in_hess, ctx.parent_class.buffer_dev, op=ReduceOp
            .AVG)

            if is_buffer:
                ctx.parent_class.hin.add_(in_hess.to(ctx.parent_class.hin.device).to(
                    op_dtype))
                ctx.parent_class.ct += bs / ctx.parent_class.scale
            if div:
                ctx.parent_class.hin.div_(ctx.parent_class.ct)
                ctx.parent_class.ct = 0

            del in_hess
            torch.cuda.empty_cache()
        else:
            if it % 2 == 0:
                if reset and is_buffer:
                    ctx.parent_class.hin.mul_(0)

                if not is_buffer:
                    out_hess = torch.zeros(ctx.parent_class.out_features * (ctx.
parent_class.out_features + 1)//2, dtype=op_dtype, device=local_rank)
                else:
                    out_hess = ctx.parent_class.hout.to(local_rank)

```

```

        torch.distributed.broadcast(out_hess, ctx.parent_class.buffer_dev)
        out_hess = flat_to_sym(out_hess, ws[0]).float()
        in_hess = input.T @ (input * ((grad_output @ out_hess) * grad_output)).
        sum(dim=-1, keepdim=True)) / out_hess.norm()**2
        del input, grad_output, out_hess
        in_hess = sym_to_flat(in_hess) / ctx.parent_class.scale
        torch.distributed.reduce(in_hess, ctx.parent_class.buffer_dev, op=
        ReduceOp.AVG)
        if is_buffer:
            ctx.parent_class.hin.add_(in_hess.to(ctx.parent_class.hin.device)).
            to(op_dtype))
            ctx.parent_class.ct += bs / ctx.parent_class.scale
            if div:
                ctx.parent_class.hin.div_(ctx.parent_class.ct)
                ctx.parent_class.ct = 0

            del in_hess
        else:
            if reset and is_buffer:
                ctx.parent_class.hout.mul_(0)

            if not is_buffer:
                in_hess = torch.zeros(ctx.parent_class.in_features * (ctx.
                parent_class.in_features + 1)//2, dtype=op_dtype, device=local_rank)
            else:
                in_hess = ctx.parent_class.hin.to(local_rank)
                torch.distributed.broadcast(in_hess, ctx.parent_class.buffer_dev)
                in_hess = flat_to_sym(in_hess, ws[1]).float()
                out_hess = grad_output.T @ (grad_output * ((input @ in_hess) * input)).
                sum(dim=-1, keepdim=True)) / in_hess.norm()**2
                del input, grad_output, in_hess
                out_hess = sym_to_flat(out_hess) / ctx.parent_class.scale
                torch.distributed.reduce(out_hess, ctx.parent_class.buffer_dev, op=
                ReduceOp.AVG)
                if is_buffer:
                    ctx.parent_class.hout.add_(out_hess.to(ctx.parent_class.hout.
                    device).to(op_dtype))
                    ctx.parent_class.ct += bs / ctx.parent_class.scale
                    if div:
                        ctx.parent_class.hout.div_(ctx.parent_class.ct)
                        ctx.parent_class.ct = 0

                del out_hess

            torch.cuda.empty_cache()
        return grad_input.to(local_rank), None, None, None
    
```

A.9 MODIFIED BACKWARD PASS TO COMPUTE SKETCH B

```

class LinearNoBias(torch.autograd.Function):
    @staticmethod
    @torch.amp.custom_fwd(device_type='cuda')
    def forward(ctx, input, weight, mode, parent_class):
        ctx.save_for_backward(input, weight)
        ctx.mode = mode
        ctx.parent_class = parent_class

        return input @ weight.T

    @staticmethod
    @torch.amp.custom_bwd(device_type='cuda')
    def backward(ctx, grad_output):
        it, reset, div = ctx.mode
        is_buffer = local_rank == ctx.parent_class.buffer_dev

        input, weight = ctx.saved_tensors
        ws = weight.shape
        grad_input = grad_output @ weight
        del weight

        if ctx.parent_class.collect_hess:
            op_dtype = ctx.parent_class.op_dtype
            bs = input.shape[0]
            with torch.amp.autocast('cuda', enabled=False):
                if it == 0:
                    if reset and is_buffer:
                        ctx.parent_class.hin.mul_(0)

            grad_output = grad_output.float()
    
```

```

        input = input.float()
        in_hess = sym_to_flat(torch.einsum('btm,btn,bsm,bsk->nk', grad_output,
input, grad_output, input))
        handle_in = torch.distributed.reduce(in_hess, ctx.parent_class.buffer_dev,
op=ReduceOp.AVG, async_op=True)
        out_hess = sym_to_flat(torch.einsum('btm,btn,bsk,bsn->mk', grad_output,
input, grad_output, input))
        handle_out = torch.distributed.reduce(out_hess, ctx.parent_class.
buffer_dev, op=ReduceOp.AVG, async_op=True)
        del grad_output, input
        handle_in.wait()
        handle_out.wait()

        if is_buffer:
            ctx.parent_class.hin.add_(in_hess.to(ctx.parent_class.hin.device).to(
op_dtype))
            ctx.parent_class.hout.add_(out_hess.to(ctx.parent_class.hout.device).
to(op_dtype))
            ctx.parent_class.ct += bs
            if div:
                ctx.parent_class.hin.div_(ctx.parent_class.ct)
                ctx.parent_class.hout.div_(ctx.parent_class.ct)
                ctx.parent_class.ct = 0

        del in_hess, out_hess
        torch.cuda.empty_cache()

    torch.cuda.empty_cache()
    return grad_input.to(local_rank), None, None, None

```

A.10 ADDITIONAL RESULTS

Table 7 contains full zeroshot results from the “no finetuning” table in the main body. Table 5 contains results comparing YAQA to CBQ, an older method that performs AdaRound-style rounding over a “sliding window” of decoder blocks. This allows it to capture cross-block dependencies beyond the immediate activation error. CBQ performs well, but is limited to scalar quantizers and is outperformed by YAQA. Another similar method, PV-Tuning, performs decoder block level quantization on the end-to-end error. PV-Tuning relies on learned vector quantizers, but is less effective on larger models. Furthermore, there are no PV-Tuned models with “standard” quantizers to compare against. However, LDLQ with a fixed trellis quantizer already outperforms PV-Tuning, so by association, so does YAQA. Finally, Table 6 shows an experiment without incoherence processing. All quantized models in this table use an INT4 quantizer with a 16 bit groupwise absmax scale shared across 32 contiguous elements, giving an effective 4.5 bits per weight. We used $g_x = 1$ and $g_y = 32$ for all methods. Even with out incoherence processing, YAQA outperforms LDLQ.

Table 5: Results without finetuning on Llama 2 7B.

| ALGORITHM | INT2 | | INT3 | | INT4 | |
|-----------|-------------|-------------|-------------|-------------|-------------|-------------|
| | W2 | C4 | W2 | C4 | W2 | C4 |
| CBQ | 8.01 | 11.30 | 5.89 | 7.56 | 5.52 | 7.05 |
| YAQA-B | 7.45 | 9.22 | 5.82 | 7.38 | 5.54 | 7.04 |

Table 6: Results without incoherence processing. All results are without finetuning and use an INT4 quantizer with a 16-bit groupwise scale shared across 32 contiguous elements (4.5 bits).

| ALGO. | $D_{KL} \downarrow$ | | $PPL \downarrow$ | | 0-SHOT ACC \uparrow | | | | | |
|--------|---------------------|-------------|------------------|--------------|-----------------------|-------|-------|-------|-------|--|
| | W2 | W2 | C4 | Avg | ARCC | ARCE | BOOLQ | HSWAG | PiQA | |
| BF16 | 0 | 6.50 | 8.02 | 69.82 | 51.37 | 78.03 | 82.05 | 57.74 | 79.92 | |
| LDLQ | 0.033 | 6.75 | 8.21 | 68.35 | 49.74 | 77.36 | 78.35 | 56.83 | 79.49 | |
| YAQA-A | 0.025 | 6.67 | 8.17 | 69.36 | 49.74 | 77.65 | 81.62 | 57.16 | 80.63 | |
| YAQA-B | 0.021 | 6.65 | 8.15 | 68.95 | 50.68 | 78.20 | 79.72 | 57.06 | 79.11 | |

Table 7: Full zeroshot accuracy results for Table 1. Higher is better.

| MODEL | ALGO. | QUANT. | 0-SHOT ACC \uparrow | | | | |
|-----------------|--------|--------|-----------------------|-------|-------|-------|-------|
| | | | ARCC | ARCE | BOOLQ | HSWAG | PIQA |
| 3.1 70B INST | LDLQ | BF16 | 56.40 | 75.34 | 62.20 | 61.51 | 82.92 |
| | | QTIP 2 | 52.05 | 73.91 | 62.17 | 58.10 | 81.01 |
| | | QTIP 3 | 56.06 | 75.88 | 62.23 | 61.00 | 82.70 |
| | | QTIP 4 | 55.72 | 75.63 | 62.29 | 61.18 | 83.08 |
| | YAQA-A | QTIP 2 | 52.82 | 74.07 | 62.17 | 58.27 | 82.26 |
| | | QTIP 3 | 56.07 | 75.88 | 62.20 | 61.84 | 82.46 |
| | | QTIP 4 | 56.06 | 75.42 | 62.17 | 61.11 | 82.75 |
| | YAQA-B | QTIP 2 | 54.44 | 73.44 | 62.17 | 59.24 | 81.66 |
| | | QTIP 3 | 55.72 | 74.33 | 62.17 | 60.91 | 83.08 |
| | | QTIP 4 | 56.31 | 76.09 | 62.29 | 61.10 | 82.86 |
| | LDLQ | BF16 | 51.37 | 78.03 | 82.05 | 57.74 | 79.92 |
| | | QTIP 2 | 41.89 | 74.28 | 67.98 | 51.67 | 76.71 |
| | | QTIP 3 | 50.34 | 77.61 | 82.05 | 56.57 | 79.87 |
| | | QTIP 4 | 50.68 | 78.07 | 80.98 | 57.32 | 79.98 |
| 3.1 8B INST | YAQA-A | QTIP 2 | 45.39 | 73.91 | 70.34 | 52.59 | 78.07 |
| | | QTIP 3 | 49.83 | 77.23 | 81.76 | 56.85 | 79.76 |
| | | QTIP 4 | 50.34 | 78.32 | 82.45 | 57.35 | 79.65 |
| | YAQA-B | QTIP 2 | 44.20 | 75.08 | 70.64 | 52.91 | 78.78 |
| | | QTIP 3 | 51.02 | 77.86 | 81.04 | 57.24 | 79.38 |
| | | QTIP 4 | 50.94 | 78.49 | 82.02 | 57.47 | 79.98 |
| | BF16 | BF16 | 44.45 | 71.42 | 76.18 | 51.19 | 75.73 |
| | | QTIP 2 | 32.00 | 58.50 | 69.42 | 45.57 | 72.91 |
| | | QTIP 3 | 41.72 | 70.66 | 74.19 | 50.46 | 75.24 |
| | | QTIP 4 | 43.52 | 71.80 | 75.93 | 51.03 | 76.22 |
| | YAQA-A | QTIP 2 | 38.65 | 66.46 | 66.76 | 45.98 | 73.61 |
| | | QTIP 3 | 42.15 | 69.70 | 74.92 | 50.04 | 75.73 |
| | | QTIP 4 | 42.66 | 70.24 | 76.57 | 50.85 | 76.06 |
| | YAQA-B | QTIP 2 | 38.05 | 68.22 | 68.75 | 47.11 | 73.39 |
| | | QTIP 3 | 42.75 | 69.95 | 75.66 | 50.38 | 74.97 |
| | | QTIP 4 | 43.60 | 71.04 | 75.96 | 50.74 | 75.19 |
| 3.2 3B INST | LDLQ | BF16 | 32.85 | 57.24 | 66.09 | 44.74 | 73.01 |
| | | QTIP 2 | 27.30 | 51.60 | 61.71 | 38.66 | 68.72 |
| | | QTIP 3 | 29.44 | 54.42 | 65.47 | 43.31 | 71.82 |
| | | QTIP 4 | 30.46 | 54.76 | 65.84 | 43.70 | 72.58 |
| | YAQA-A | QTIP 2 | 27.59 | 51.55 | 62.84 | 39.28 | 68.86 |
| | | QTIP 3 | 32.17 | 56.02 | 65.47 | 43.51 | 72.14 |
| | | QTIP 4 | 32.51 | 56.86 | 64.37 | 44.33 | 72.80 |
| | YAQA-B | QTIP 2 | 27.47 | 54.46 | 62.51 | 39.89 | 70.18 |
| | | QTIP 3 | 31.31 | 56.44 | 62.60 | 43.20 | 73.50 |
| | | QTIP 4 | 31.48 | 55.18 | 64.86 | 43.42 | 74.27 |